Investigations on the mixed Jahn-Teller system (Tb_x, Dy_{1-x})VO_4. I. Phase diagram, specific heat and spectroscopic measurements

1990 J. Phys.: Condens. Matter 2 1073

(http://iopscience.iop.org/0953-8984/2/5/003)

J. Phys.: Condens. Matter **2** (1990) 1073–1095. Printed in the UK

Investigations on the mixed Jahn–Teller system $(Tb_x,Dy_{1-x})VO_4$: I. Phase diagram, specific heat and spectroscopic measurements

G Hess, M Dammann, H G Kahle, A Kasten†, C Seifert and K Vögtlin
Physikalisches Institut, Universität Karlsruhe (TH), PO Box 6980, D-7500 Karlsruhe 1, Federal Republic of Germany

Received 2 May 1989, in final form 22 August 1989

Abstract. At low temperatures $TbVO_4$ and $DyVO_4$ exhibit a structural phase transition from the same high-temperature structure to different low-temperature structures. Owing to symmetry, different crystallographic domains are possible. Investigations of single crystals of the mixed system $(Tb_x,Dy_{1-x})VO_4$ with a polarising microscope gave information about domain distribution and distortion type. Specific heat measurements, spectroscopic and birefringence data yielded the transition temperatures. The phase diagram of the mixed system may be interpreted as a superposition of the phase diagram of diluted $TbVO_4$ and that of diluted $DyVO_4$. At high concentrations of one of the rare-earth ions the crystals distort like the respective pure substances, whereas at medium concentrations $x \simeq 0.4$ a superposition of the distortion types is observed. The measurements are interpreted in the frame of a mean-field approximation, which is modified by the phenomenological compressible Ising model and by the inclusion of local strains of random distribution.

1. Introduction

$TbVO_4$ and $DyVO_4$ belong to a series of isostructural rare-earth compounds exhibiting a structural phase transition caused by the cooperative Jahn–Teller effect (CJTE) [1]. While the high-temperature structures of these two compounds are the same (tetragonal zircon structure, space group $I4_1/amd$ [2]), apart from slightly different lattice constants, their low-temperature structures are different. $DyVO_4$, for $T < T_D \simeq 14$ K, distorts parallel to the tetragonal $\boldsymbol{a}$ or $\boldsymbol{b}$ axis to its low-temperature structure $Imma$ [3–5]. $TbVO_4$, on the contrary, for $T < T_D \simeq 33$ K, distorts parallel to one of the bisectrices of the $\boldsymbol{a}$ and $\boldsymbol{b}$ axes [4, 6], henceforth called $\boldsymbol{x}$ and $\boldsymbol{y}$ axes. Its low-temperature structure is thus $Fddd$.

The order parameters of the phase transitions are proportional to the respective macroscopic distortion, which we designate

$$e_A = e_{11} - e_{22} = \Delta a/a - \Delta b/b \qquad \text{for } DyVO_4$$

and

$$e_X = 2e_{12} = \Delta x/x - \Delta y/y \qquad \text{for } TbVO_4$$

with e_{ij} the components of the strain tensor [7]. The distortions are different in their

† Present address: Bruker Analytische Messtechnik, D-7512 Rheinstetten, Federal Republic of Germany.

0953-8984/90/051073 + 23 $03.50

transformation properties with respect to the irreducible representations of the point group 4/mmm of the high-temperature phase. We use the notation of [8] and designate the distortion type of $DyVO_4$ as Γ_4^+ and that of $TbVO_4$ as Γ_3^+. Other authors, e.g. Elliott *et al* [9], used the spectroscopic notation B_{1g} for $DyVO_4$ and B_{2g} for $TbVO_4$. Because of the equivalence of the tetragonal ***a*** and ***b*** directions, crystallographic domains occur in $DyVO_4$ as well as in $TbVO_4$. The domain walls are at 45° to the distortion direction; thus observation of the domain structure gives a hint of the distortion type.

The mechanism of the phase transition has been studied experimentally and theoretically with several methods. For a review of the first investigations see Gehring and Gehring [1]. Later publications include studies of birefringence [10, 11], specific heat [12] and dielectric constants [13].

Further investigations were made possible by measurements on mixed systems. All rare-earth vanadates (and arsenates) have similar lattice parameters and can be mixed in arbitrary ratios. By partial substitution of the Jahn–Teller (JT)-active rare-earth ion by an inactive one, e.g. by Gd^{3+}, Lu^{3+} or Y^{3+}, the effective coupling between the active ions can be reduced [14–18]. If two rare-earth ions both of which are JT-active and give the same distortion type (e.g. $TbVO_4$ and $TmVO_4$ [19, 20] or $TbAsO_4$ and $TmAsO_4$ [19, 20]) are mixed, the situation gets complicated because of coupling of the two ions via a common strain.

The temperature dependence of the order parameter and the specific heat were published only for mixtures distorting like $TbVO_4$ [14, 17, 19, 20]. For mixtures containing Dy^{3+}, only the transition temperatures (and some dielectric data) are known [15, 18, 21]. The different ionic radii lead to a statistical distribution of the two rare-earth ions in the mixed crystals and consequently to a non-homogeneous macroscopic strain [16, 17, 19, 21]. Not only cation mixtures but also anion mixtures are possible, e.g. $DyVO_4$ and $DyAsO_4$, which were studied successfully [21, 22].

This publication reports on the phase diagram of the mixed system $(Tb_x,Dy_{1-x})VO_4$ and on specific heat and optical measurements. The distortion type was ascertained by means of crystal optical methods. The transition temperatures were determined by specific heat and birefringence measurements. Details of the birefringence experiments will be published in the two following papers [23, 24], which henceforth will be designed as II and III, respectively. Additionally, we report on measurements of absorption spectroscopy giving information about the eigenvalues of the Hamiltonian. Preliminary results on $(Tb_x,Dy_{1-x})VO_4$ were published in the Proceedings of the ICM 1988 [25].

2. Experimental details

2.1. Samples

The crystals were flux-grown in the Kristall- und Materiallabor der Fakultät für Physik der Universität Karlsruhe [26]. In addition to the pure substances ($x = 0.0$ and $x = 1.0$), mixed crystals with $x = 0.1, 0.2, \ldots, 0.9$ and $x = 0.35$ and 0.45 were grown. The accuracy of the concentrations was verified with atomic absorption spectroscopy to 2% of the rare earth that is predominant.

In the crystal optical, specific heat and spectroscopic measurements, different crystals of the same batch were used for each concentration x. For $x = 0.4$, two samples (I and II) of different batches were measured in the specific heat experiments. Sample II was also used for the birefringence measurements. The crystals for the crystal optical

measurements were cut perpendicular to the tetragonal ***c*** axis and polished. The crystals for the specific heat experiments and spectroscopic measurements were used as-grown. In the specific heat experiments batches of up to four crystals with a total mass of about 0.2 g were measured.

2.2. Crystal optical measurements

These experiments were carried out in a gas-flux cryostat. The temperature was measured by a calibrated carbon resistor. To produce single-domain crystals, magnetic fields up to $B = 0.2$ T were applied by a conventional electromagnet. The crystal was placed between crossed polarisers, the polarising direction being parallel to the tetragonal ***a*** or ***b*** direction or parallel to the ***x*** or ***y*** direction. The light source was a Xe high-pressure lamp.

Domain distributions make themselves conspicuous by different colours in the interference pattern, which was projected onto a screen. Using the conoscopic light path (convergent light), the optical indicatrix was determined [27]. This allowed conclusions about the symmetry of the distortion. The light for these investigations was monochromatised by interference filters (λ = 436, 547, 578 and 653 nm) and focused onto the crystal.

2.3. Specific heat experiments

The specific heat experiments were carried out in a ^{4}He bath cryostat using the conventional heat-pulse method. Corrections were made to account for the heat capacity of sample holder, heater and thermometer and the lattice contribution to the specific heat with a Debye temperature of $\Theta_D = 250$ K. For details, we refer to [19].

2.4. Spectroscopic measurements

The measurements of absorption spectroscopy were carried out in a gas-flux cryostat with a carbon-resistor thermometer. The crystal was irradiated perpendicular to the ***c*** axis with white light from a Xe high-pressure lamp. The spectra were taken in a 3.4 m Jarrell–Ash Ebert spectrograph with a theoretical resolution (limited by the entrance and exit slits) of $\Delta\tilde{\nu} = 0.22$ cm^{-1} in the measured region. The real resolution was worse because of the finite linewidth (about 1 cm^{-1}). The spectra were recorded automatically by data processing using a photomultiplier mounted onto a step-driven slide. The scanning region was 10 cm at maximum, corresponding to a wavenumber interval of about 400 cm^{-1}.

Transitions of the Tb^{3+} ions from the ground term $^7F_6$ to the term $^5D_4$ and transitions of the Dy^{3+} ions from the ground term $^6H_{15/2}$ to the term $^4F_{9/2}$ were investigated. From measurements in σ and π polarisation the ground states (lowest four crystal-field states) were determined.

3. Distortion type and phase diagram

3.1. Distortion type

3.1.1. Dy-rich crystals ($0.0 \leq x \leq 0.3$). In the orthoscopic light path, Dy-rich crystals show the same domain structure as $DyVO_4$ [8, 28–30]. The domain walls are parallel to

x and y, i.e. at 45° to the two possible distortion directions parallel to a and b. The domains have dimensions of about $15 \times 30\ \mu m^2$ in the (a, b) plane. In a magnetic field of $B \simeq 0.2$ T in the distortion direction, the domain structure disappears and the crystals become single-domained. In a field $B \parallel x$, i.e. at 45° to the distortion direction, domain walls perpendicular to the magnetic field are observed as in pure $DyVO_4$ [29, 30]. The conoscopic interference pattern is typical for an orthorhombic structure with axes parallel to the tetragonal a and b directions.

3.1.2. Tb-rich crystals ($0.45 \leq x \leq 1.0$). Tb-rich crystals behave as pure $TbVO_4$. The domain structure is the same as in $TbAsO_4$ [31]. The domain walls are parallel to a and b, i.e. at 45° to the distortion direction. The regions of equal interference colours are much broader (about 300 μm) than for the Dy-rich compounds. As before, the domains can be removed by a magnetic field of $B \simeq 0.2$ T in the distortion direction. The conoscopic interference pattern is typical for an orthorhombic structure with axes parallel to x and y.

3.1.3. Intermediate concentrations ($x = 0.35$ and $x = 0.4$). For intermediate concentrations, depending on temperature, at $B = 0$ T both domain types are observed. Below the lower transition temperature T_{D2}, the domain structure of $DyVO_4$ is observed. Additionally, in the sample with $x = 0.4$ wavy stripes along a appear. For $T \simeq T_{D2}$ additional stripes parallel to x and y can be seen and the stripes along a become more indistinct. For $T_{D2} \leq T \leq T_{D1}$ the domain structure of $TbVO_4$ is present.

In magnetic fields parallel to the main distortion directions (a, b, x or y), the corresponding domain structures of the pure substances are observed [32]. For these four field directions there is always a temperature range where domains exist. In a field that is parallel to the bisectrix of the a and x axes, however, i.e. at 22.5° to the a axis, the crystals are single-domained in all phases. For $T < T_{D2}$ a dispersion of the indicatrix axes in the conoscopic interference pattern is observed. This dispersion is characteristic for crystals with monoclinic (or triclinic) symmetry. It is caused by the superposition of the two Jahn–Teller distortion types Γ_3^+ (parallel to x) and Γ_4^+ (parallel to a) and the different birefringence dispersions for the two distortion types. For details of the birefringence and its dispersion, we refer to paper II and to [33]. With increasing temperature, the indicatrix rotates towards the x axis. For the blue region of the spectrum, the x axis is reached already at lower temperatures than for the longer wavelengths, since the elasto-optical coefficient [7] for the Γ_3^+ distortion is very much smaller in the long-wavelength than in the blue region. For longer wavelengths the influence of the Γ_4^+ distortion on the indicatrix is preserved to higher temperatures although the Γ_4^+ distortion is smaller than the Γ_3^+ distortion. The macroscopic superposition of the two distortion types, as observed here, is confirmed by birefringence measurements which agree with a calculation including the consequences of this superposition (see paper III).

3.2. Phase diagram

Figure 1 shows the phase diagram of $(Tb_x,Dy_{1-x})VO_4$ determined from the maxima of the specific heat (§ 5). For comparison, the values of T_D determined from birefringence measurements (extreme values of $d(\delta n)/dT$ in magnetic field and extrapolation to $B = 0$; see paper II) are given. In table 1 the transition temperatures are listed together with the measured and calculated jumps of the molar specific heat (for the calculations, see § 5). The discrepancies in the values of T_D for the Γ_3^+ distorted crystals with great x have

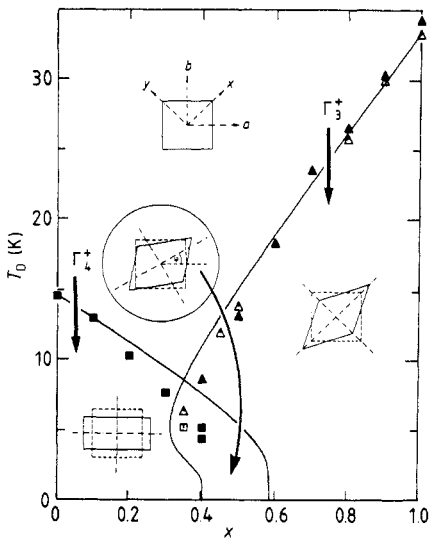

Figure 1. Phase diagram of the structural phase transitions of $(Tb_x,Dy_{1-x})VO_4$. Squares: Γ_4^+ transitions (Dy type). Triangles: Γ_3^+ transitions (Tb type). Full symbols: taken from specific heat measurements (this paper). Open symbols: taken from birefringence measurements (paper II). Full curves: T_D in mean-field approximation. The respective distortion type is drawn symbolically in the phases.

Table 1. Transition temperatures T_D and specific heat data of $(Tb_x,Dy_{1-x})VO_4$.

Tb concentration, x	Crystallographic transition temperature, T_D (K)			Jump, $\Delta C/R$		Néel temperature, T_N (K)
	Specific heat (this paper)	Birefringence (paper II)	Spectroscopy (this paper)	Experiment[a]	Theory	Specific heat
Γ_3^+ distorted crystals						
1.0	34.3 ± 0.1	33.3 ± 0.4	33.2 ± 0.2	1.2 ± 0.2	1.42	—
0.9	30.4 ± 0.1	30.0 ± 0.4	29.4 ± 0.3	1.1 ± 0.2	1.17	—
0.8	26.6 ± 0.1	25.8 ± 0.4	26.5 ± 0.3	0.90 ± 0.15	0.96	—
0.7	23.6 ± 0.1	23.3 ± 0.3	22.5 ± 0.5	0.71 ± 0.05	0.84	—
0.6	18.4 ± 0.1	18.4 ± 0.3	18.5 ± 0.5	0.44 ± 0.05	0.56	—
0.5	13.2 ± 0.2	13.2 ± 0.2	14.0 ± 0.5	0.32 ± 0.05	0.28	—
0.45	—	12.0 ± 0.2	—	—	—	—
0.4[b]	8.7 ± 0.1	—	8.5 ± 0.5	0.11 ± 0.03	0.08	—
0.4[c]	9.0 ± 0.2	9.0 ± 0.1	—	0.10 ± 0.03	0.08	—
0.35	—	6.4 ± 0.2	—			—
Γ_4^+ distorted crystals						
0.0	14.6 ± 0.1	14.5 ± 0.2	15.0 ± 0.5	2.47 ± 0.10	2.63	3.05 ± 0.05
0.1	13.0 ± 0.1	12.8 ± 0.2	13.2 ± 0.5	1.78 ± 0.08	1.86	2.75 ± 0.05
0.2	10.3 ± 0.1	10.3 ± 0.2	10.5 ± 0.5	0.85 ± 0.05	0.92	2.40 ± 0.05
0.3	7.7 ± 0.1	7.6 ± 0.1	7.8 ± 0.5	0.45 ± 0.05	0.43	1.95 ± 0.05
0.35	—	5.2 ± 0.1	—	—	—	—
0.4[b]	4.4 ± 0.2	—	$2 \leqslant T_D \leqslant 5$	0.03 ± 0.01	0.04	1.50 ± 0.05
0.4[c]	5.2 ± 0.1	5.2 ± 0.1	—	0.10 ± 0.01	0.12	1.52 ± 0.05
0.45	—	<2.1	—	—	—	—
0.5	<1.1	<1.5	<1.5	—	—	1.35 ± 0.05

[a] With high-temperature tail extrapolated to T_{D2}.
[b] Sample I (see § 5.3.2).
[c] Sample II (see § 5.3.2).

also been observed in $(Tb_x,Tm_{1-x})VO_4$ and $(Tb_x,Tm_{1-x})AsO_4$ [19]. The value of T_D for $x = 0.7$ is too high compared with those of the neighbouring concentrations. It is also too high compared with mean-field approximation (MFA). According to the calculations, the real concentration in the measured samples must be at least 0.71. The difference of the Γ_4^+ transition temperatures of the two samples with $x = 0.4$ is presumably due to different random strains in these samples (see § 5.3.2).

The transition temperatures found for the $(Tb_x,Dy_{1-x})VO_4$ system deviate distinctly less from the mean-field values than those of the other mixed systems containing either $TbVO_4$ or $DyVO_4$ [15, 18, 19] (with the exception of $(Y_x,Dy_{1-x})VO_4$ [15]). Obviously, the deviation depends on the difference of the ionic radii of the mixed rare-earth ions or on the difference of the lattice parameters of the pure substances, respectively.

The phase diagram as a whole is an undisturbed superposition of the phase diagram of $TbVO_4$ diluted with Dy^{3+} and that of $DyVO_4$ diluted with Tb^{3+}. For the measured samples with $x = 0.35$ and $x = 0.4$, the two distortion types are superimposed, as shown by crystal optical measurements (§ 3.1.3.) and birefringence measurements (see paper III). This yields a macroscopic monoclinic distortion and a space group $C2/c$ for these crystals for $T < T_{D2}$. In mean-field approximation (see § 4) a tetracritical point is obtained where the two phase boundaries intersect.

A similar superposition of phase transitions due to competing interaction mechanisms is known both in mixed Jahn–Teller spinels [34–36] and in mixed antiferromagnets, where the pure substances have different easy axes [37], leading to an intermediate phase designated as 'mixed order antiferromagnet' [38] or 'oblique antiferromagnet' [39]. We confine ourselves to a comparison with the magnetic systems because the order parameter in the spinel system is two-dimensional even in the pure substances [40] leading to a different interpretation of the mixed system [41] compared to that of systems where the order parameter of the pure substances is one-dimensional.

Two points in the discussion of mixed antiferromagnets are of interest for our system:

The first one is the behaviour of the phase transitions in the vicinity of the tetracritical point. Owing to renormalisation-group theory [38, 42], the phase boundaries of the diluted antiferromagnets intersect without discontinuity at the tetracritical point. According to Landau theory [43] and correspondingly in mean-field approximation [39], this is the case only if there is no cross term in the free energy, i.e. if there is no interaction between the magnetic moments of the two mixed ions or if there are no off-diagonal terms in the Hamiltonian. This is approximately realised, for example, in $(Fe_x,Co_{1-x})Cl_2 \cdot 2H_2O$ [44–46]. Transferring these results to our Jahn–Teller system, we note that in both pure $TbVO_4$ and $DyVO_4$ the interaction constants related to the respective distortion type of the other rare-earth ion are small compared with those of the 'own' ion [9]. This is in accordance with the experimental phase diagram of the mixed system. The Γ_4^+ transition temperature of $(Tb_{0.35},Dy_{0.65})VO_4$ (figure 1) does not argue against that because internal strains can lower the transition temperature, as demonstrated in the two samples with $x = 0.4$ (see § 5.3.2).

The second point is the sharpness of the lower transition temperature. In the mixed Ising-xy antiferromagnet $(Fe_x,Co_{1-x})Cl_2$, the transition at the lower temperature is smeared out while that at the higher temperature remains sharp [47, 48]. This was explained with random-field effects due to off-diagonal terms in the Hamiltonian. In $(Tb_{0.4},Dy_{0.6})VO_4$, the lower (i.e. Γ_4^+) transition is sharp in both specific heat (§ 5.3.2) and birefringence experiments (cf figure 6(*b*) of paper II). Thus the absence of cross terms in the interactions is supported.

4. Theory

4.1. Mean-field approximation

The theoretical description of the cooperative Jahn–Teller effect (CJTE) in the rare-earth zircons is based upon the pseudo-spin formalism and the corresponding mean-field approximation, developed by Elliott *et al* [9]. It considers a pseudo-spin–pseudo-spin interaction and a coupling of the pseudo-spins to the macroscopic distortion. In mean-field approximation (MFA) the pseudo-spin–pseudo-spin interaction reads $\lambda\langle\sigma^z\rangle\sigma^z$, and the coupling to the macroscopic strain reads $\eta e\sigma^z$. Here $\langle\sigma^z\rangle$ is the configuration average of the pseudo-spin operator σ^z, e is the macroscopic distortion ($e = e_X$ for $TbVO_4$, $e = e_A$ for $DyVO_4$), λ is the interaction constant of the pseudo-spins and η is the coupling constant with the distortion. The configuration average $\langle\sigma^z\rangle$ acts as an order parameter of the Jahn–Teller (JT) transition.

For a theoretical description, knowledge of the crystal-field states is necessary. These have been determined by optical spectroscopy and Raman scattering [8, 9, 28, 49, 50]. In $TbVO_4$, at low temperatures but $T > T_D$, four crystal-field states are occupied: a singlet (Γ_1) at $-\varepsilon$, a doublet (Γ_5) at ε' and another singlet (Γ_3) at $+\varepsilon$. In $DyVO_4$, two Kramers doublets (Γ_6 and Γ_7) are occupied with a distance $2\Delta_0$ for $T > T_D$.

The mean-field Hamiltonians for $TbVO_4$ and $DyVO_4$ in an arbitrary magnetic field and their eigenvalues W_i have been given by McPherson *et al* [51] and Pytte [52]. For the self-consistent calculation of the distortion, the partition function

$$Z = \sum_{i=1}^{4} \exp(W_i/kT) = Z(\lambda\langle\sigma^z\rangle + \eta e) \tag{1}$$

is needed. Apart from the crystal-field parameters, it only depends on the sum $(\lambda\langle\sigma^z\rangle + \eta e)$, for both substances in the stress-free case.

4.1.1. General considerations for diluted systems. The experimental results showed that the phase diagram of the mixed system $(Tb_x,Dy_{1-x})VO_4$ is a superposition of the phase diagrams of the two diluted pure substances. In the following equations the concentration of the JT-active ion is denoted as x, which means x_{Tb} or x_{Dy}, respectively, and that of the JT-inactive ion is denoted as $(1 - x)$, which means, for example, $1 - x_{Tb} = x_{Dy}$.

The partition function of the JT-active ion is a function of $(x\lambda\langle\sigma^z\rangle + \eta e)$, i.e.

$$Z_{\text{active}} = Z_{\text{active}}(x\lambda\langle\sigma^z\rangle + \eta e) \tag{2}$$

while the partition function of the inactive ion does not depend on this variable. The free energy related to one rare-earth ion is thus

$$F = -xkT \ln Z_{\text{active}}(x\lambda\langle\sigma^z\rangle + \eta e) - (1 - x)kT \ln Z_{\text{inactive}} + \tfrac{1}{2}x^2\lambda\langle\sigma^z\rangle^2 + \tfrac{1}{2}V_0c_0e^2. \tag{3}$$

Here $V_0 = \frac{1}{4}abc$ is the effective volume of a rare-earth ion and c_0 is the elastic constant for $T \to \infty$ ($c_0 = c_X \equiv c_{66}$ for $TbVO_4$, $c_0 = c_A \equiv \frac{1}{2}(c_{11} - c_{12})$ for $DyVO_4$).

The order parameter $\langle\sigma^z\rangle$ and the distortion e can be calculated using the relations for thermodynamic equilibrium

$$\partial F/\partial\langle\sigma^z\rangle = 0 \tag{4}$$

and

$$\partial F/\partial e = 0 \tag{5}$$

leading to implicit equations for $\langle\sigma^z\rangle$ and e, respectively. From equation (3) it follows that $\langle\sigma^z\rangle$ and e are proportional [52], with

$$e = x\frac{\eta}{V_0 c_0}\langle\sigma^z\rangle. \tag{6}$$

Therefore, $\langle\sigma^z\rangle$ and e may be regarded as equivalent order parameters. The total interaction constants can be related either to $\langle\sigma^z\rangle$ or to e as

$$x\lambda\langle\sigma^z\rangle + \eta e = x(\lambda\langle\sigma^z\rangle + \mu\langle\sigma^z\rangle) = xJ_0'\langle\sigma^z\rangle = H_0' e. \tag{7}$$

In this and the following papers II and III, the order parameter e is used for the following reasons. First, for the calculation of the birefringence in II, excitations of the vanadate complex must be taken into account, too. However, $\langle\sigma^z\rangle$ is defined for rare-earth ions only and not for the vanadate anion. Secondly, the pre-stains introduced in the following section explicitly are strains and therefore not immediately related to $\langle\sigma^z\rangle$. The interaction constants that are usually related to $\langle\sigma^z\rangle$ may be converted by

$$H_0' = \frac{J_0'}{\mu^{1/2}}(V_0 c_0)^{1/2} = \frac{\lambda+\mu}{\mu^{1/2}}(V_0 c_0)^{1/2} = \frac{J_0'}{\eta}V_0 c_0. \tag{8}$$

The free energy as a function of e only is then

$$F = -xkT\ln Z_{\text{active}}(H_0' e) - (1-x)kT\ln Z_{\text{inactive}} + \tfrac{1}{2}V_0 c_0 e^2(J_0'/\mu). \tag{9}$$

The additional factor (J_0'/μ) in the elastic energy comes from the conversion of the term $\frac{1}{2}x^2\lambda\langle\sigma^z\rangle^2$.

If one supposes the elastic constants c_A of $TbVO_4$ and $DyVO_4$ to be equal and if one supposes the same for c_X, the free energy becomes

$$F = F_{Tb} + F_{Dy} \tag{10}$$

with

$$F_{Tb} = -xkT\ln Z_{Tb}(H_{0,Tb}' e_X) + \tfrac{1}{2}V_0 c_X e_X^2(J_{0,Tb}'/\mu_{Tb}) \tag{11}$$

and

$$F_{Dy} = -(1-x)kT\ln Z_{Dy}(H_{0,Dy}' e_A) + \tfrac{1}{2}V_0 c_A e_A^2)(J_{0,Dy}'/\mu_{Dy}). \tag{12}$$

Analogously to equation (5) the conditions

$$\partial F/\partial e_X = 0 \tag{13}$$

and

$$\partial F/\partial e_A = 0 \tag{14}$$

lead to the implicit independent equations

$$e_X(T) = f_X(e_X, T) \tag{15}$$

and

$$e_A(T) = f_A(e_A, T). \tag{16}$$

The specific heat C is calculated as the derivative of the energy U,

$$C = C_{Tb} + C_{Dy} = dU_{Tb}/dT + dU_{Dy}/dT = dU/dT \tag{17}$$

with

$$U_{Tb} = \frac{x}{Z_{Tb}} \sum_i W_{i,Tb} \exp\left(\frac{-W_{i,Tb}}{kT}\right) + \tfrac{1}{2} V_0 c_X e_X^2 \frac{J'_{0,Tb}}{\mu_{Tb}} \tag{18}$$

and

$$U_{Dy} = \frac{1-x}{Z_{Dy}} \sum_i W_{i,Dy} \exp\left(\frac{-W_{i,Dy}}{kT}\right) + \tfrac{1}{2} V_0 c_A e_A^2 \frac{J'_{0,Dy}}{\mu_{Dy}}. \tag{19}$$

4.1.2. Random strains. The transition temperatures of the mixed systems of the rare-earth zircons investigated so far are significantly lower than the values expected in MFA [14–21]. For their explanation, several phenomenological *ansatzes* have been made. We adopt here an *ansatz* introduced by Gehring *et al* [16] and used in other publications [17, 19, 21]. A distribution of pre-strains due to the different lattice parameters of the pure substances is taken into consideration. This distribution e_v is assumed to be Gaussian with half-width $e_{1/2}$,

$$p(e_v) \sim \exp(-e_v^2 \ln 2/e_{1/2}^2) \tag{20}$$

and e_v has the same symmetry (Γ_3^+ or Γ_4^+) as the respective distortion. The following considerations are valid for diluted $TbVO_4$ and for diluted $DyVO_4$ as well as for the region where both distortion types superimpose. In order to reproduce the smearing-out of the phase transition in the specific heat, even for measurements without magnetic field, an additional small pre-strain e_s was assumed, making the pre-strain distribution unsymmetrical [19]. Then $p(e_v)$ becomes

$$p(e_v) \sim \exp[-(e_v + e_s)^2 \ln 2/e_{1/2}^2]. \tag{20a}$$

Similar effects are produced by a Γ_5^+ strain or a distribution of local concentration gradients. It can be shown that, for the case of a Gaussian distribution of pre-strains, $\langle\sigma^z\rangle$ and e are still proportional and equation (6) remains valid. The free energy, (11) or (12) respectively, becomes

$$F(e) = \int F_0(e, e_v) p(e_v)\, de_v \tag{21}$$

with the term $(x\lambda\langle\sigma^z\rangle + \eta e)$ in the free energy F_0 replaced by

$$(x\lambda\langle\sigma^z\rangle + \eta e + \eta e_v) = (H'_0 e + \eta e_v). \tag{22}$$

It is important that the effective interaction constants H'_0 for e and η for e_v are thus different for $\lambda \neq 0$. The distortion e is calculated self-consistently in the same manner as in equations (15) and (16) by

$$e = \int f(e, e_v) p(e_v)\, de_v. \tag{23}$$

The specific heat is evaluated with $C = dU/dT$, as above, and

$$U(e_v) = \int U_0(e, e_v) p(e_v)\, de_v. \tag{24}$$

In spectroscopy, instead of the eigenvalues W_i, their averages are measured

$$\langle W_i(e)\rangle = \int W_i(e, e_v) p(e_v)\, de_v. \tag{25}$$

The interactions in $DyVO_4$ and $TbVO_4$ responsible for the CJTE are strongly anisotropic [9], thus establishing the 3D Ising character of both systems [10]. Furthermore,

$TbVO_4$ shows nearly perfect mean-field behaviour [10, 53, 54] due to its predominant coupling via $\boldsymbol{k} \simeq 0$ acoustic phonons. In the mixed substances, the inhomogeneities are obviously relatively large and the random pre-strains spatially spread to such a degree that the system will not break up into domains in the sense of Imry and Ma [55, 56]. An unsmearing of the phase transition in an external field is not observed. A small field indeed shifts the transition to higher temperatures, but produces a further smearing of the phase transition; see figure 6(*b*) of paper II. These two effects are present already without additional random pre-strains [51, 52, 57], but they are intensified with increasing dilution. This can qualitatively be understood by inspection of equation (30) (see below).

It should be mentioned that a parametrisation of disorder (as is done in this section) includes both effects of site disorder (via the occupation of the rare-earth sites by JT-inactive ions) and randomly distributed interactions (via local stress due to different lattice parameters of the pure substances). In the case of 'strong randomness', these two effects lead to very different behaviour [58–60]. A discussion of these aspects, however, would go beyond the scope of this paper.

4.2. Modifications of the MFA for $DyVO_4$ and diluted $DyVO_4$

For $DyVO_4$ and diluted $DyVO_4$, the MFA is neither capable of reproducing the full temperature dependence of the distortion (or related physical quantities) nor of yielding the experimentally determined transition temperature. The reason is that short-range interactions of the electronic states with optical phonons are effective. Therefore modifications of the MFA were necessary.

4.2.1. Rescaled MFA. In an early *ansatz* explicitly considering short-range interactions, the temperature dependence of the elastic constants was correctly reproduced for $T \geqslant T_D$ [53]. This *ansatz* could not be extended to $T < T_D$, however. Furthermore, several modifications were suggested, resulting in a rescaling of the interaction constants, or a power-series expansion of the elastic susceptibility [15]. With these modifications the transition temperatures of the mixed system $(Y_x,Dy_{1-x})VO_4$ could be explained. The system $(Gd_x,Dy_{1-x})VO_4$, however, showed the incompleteness of these models. For this system, distinctly smaller values of T_D were measured for the same dilution [18]. Further calculations considered a possible Dy–Gd interaction and a magnetostrictively induced electric quadrupole moment of the Gd^{3+} ion [18]. Both interactions were parametrised. With this modification the crystallographic transition temperature T_D of both mixed systems and the Néel temperature T_N of $(Gd_x,Dy_{1-x})VO_4$ were reproduced. Nevertheless, this *ansatz* is not satisfactory because it does not explain the temperature dependence of the order parameter of $DyVO_4$, which is approximately proportional to $(T_D - T)^{1/3}$ [10] and thus steeper as in a rescaled MFA.

4.2.2. Compressible Ising model. Another *ansatz* applied the compressible Ising model (CI model) to the structural phase transition in $DyAsO_4$ [61], which, in contrast to that of other rare-earth zircons [61, 62], is discontinuous. It states that the interaction responsible for the CJTE depends on the order parameter

$$J' = J_0'(1 + \zeta\langle\sigma^z\rangle^2). \tag{26}$$

The parameter J_0' is fitted to the experimentally determined transition temperature T_D. The introduction of the compressibility ζ changes the interaction in such a way that

the temperature dependence found for the various physical quantities is satisfactorily reproduced. At first, ζ was introduced purely phenomenologically. Later it was related to the 'effective number of interacting neighbours' z [63] and thus to the short-range character of the interaction.

Introducing the parameter ζ, the phase transition becomes steeper as in MFA and for $\zeta > \frac{1}{3}$ even discontinuous. With the CI model, the temperature dependence of the dielectric susceptibility of $DyAsO_4$ and $DyVO_4$ [13, 61] as well as those of the birefringence [11] and the specific heat [12] of $DyVO_4$ were reproduced. Details, e.g. eigenvalues in a magnetic field, may be found in [61]. The CI model leads to a restriction of the region with correct critical exponents. Outside this region, wrong exponents would be derived [11].

4.2.3. Compressible Ising model for diluted $DyVO_4$. In the applications of the CI model to $DyAsO_4$ and $DyVO_4$ published so far, the pseudo-spin–pseudo-spin interaction was assumed to be responsible for the CJTE, neglecting coupling to the elastic strains: $\eta = 0$, thus $J_0' = \lambda$. For the pure substances this does not lead to modifications, apart from a scaling of the distortion. For the diluted substances, however, distinct differences occur.

In the following, it is assumed that both the pseudo-spin–pseudo-spin interaction λ and the coupling η to the strains depend on the order parameter. With the additional assumption that λ depends on $\langle\sigma^z\rangle$ only and η depends on e_A only, the following relations are stated:

$$\lambda' = \lambda_0(1 + \zeta\langle\sigma^z\rangle^2) \tag{27}$$

$$\eta' = \eta_0(1 + \xi e_A^2). \tag{28}$$

Here ζ describes the anharmonicity of the pseudo-spin–pseudo-spin interaction and ξ the anharmonicity of the elastic energy. As in equation (2) of [12], this leads to the following relation for the free energy F_{Dy} instead of equation (12) (the magnetic field $\boldsymbol{B}$ is parallel to $\boldsymbol{a}$ and magnetic dipole and exchange fields have been neglected):

$$F_{Dy} = -x_{Dy}kT \ln Z_{Dy}(x_{Dy}\lambda'\langle\sigma^z\rangle, \eta' e_A) + \tfrac{1}{2}x_{Dy}^2\lambda_0\langle\sigma^z\rangle^2 + \tfrac{3}{4}x_{Dy}^2\zeta\lambda_0\langle\sigma^z\rangle^4 + \tfrac{1}{2}V_0c_Ae_A^2 + \tfrac{3}{4}\xi V_0c_Ae_A^4 \tag{29}$$

where $x_{Dy} = 1 - x_{Tb}$ and the partition function

$$Z_{Dy}(x_{Dy}\lambda'\langle\sigma^z\rangle, \eta' e_A) = 2\left[\exp\left(\frac{H_a}{2}\right)\cosh\left(\frac{[(S + H_a/2)^2 + \Delta^2]^{1/2}}{kT}\right) + \exp\left(\frac{-H_a}{2}\right)\cosh\left(\frac{[(S - H_a/2)^2 + \Delta^2]^{1/2}}{kT}\right)\right] \tag{30}$$

with $H_a = \frac{1}{2}g_{spectr}\mu_B B$ and

$$S = x_{Dy}\lambda_0\langle\sigma^z\rangle(1 + \zeta\langle\sigma^z\rangle^2) + \eta_0 e_A(1 + \xi e_A^2).$$

F_{Tb} is obviously not changed.

The energy U_{Dy} needed for the calculation of the specific heat can be calculated analogously to the free energy.

It should be noticed that the quantities λ' and η' in equation (30) are no longer constant parameters but depend on $\langle\sigma^z\rangle$ and e_A via equations (28) and (29).

Using equations (4) and (5), it can be shown that equation (6) is still valid. So $\langle\sigma^z\rangle$ and e_A are proportional also in this case. As in § 4.1.1 $\langle\sigma^z\rangle$ may be replaced by e_A and vice versa. In particular, the following relations hold

$$\begin{aligned} x_{Dy}\lambda_0\langle\sigma^z\rangle(1+\zeta\langle\sigma^z\rangle^2)+\eta_0 e_A(1+\xi e_A^2) \\ &= x_{Dy}J_0'\langle\sigma^z\rangle(1+\tilde{\zeta}\langle\sigma^z\rangle^2) \\ &= x_{Dy}J'\langle\sigma^z\rangle \\ &= H_0' e_A(1+\tilde{\xi}e_A^2) \\ &= H' e_A \end{aligned} \tag{31}$$

with

$$\tilde{\zeta} = \frac{\zeta\lambda_0 V_0 c_A + x_{Dy}^2\xi(J_0' - \lambda_0)}{J_0' V_0 c_A} \tag{32}$$

and

$$\tilde{\xi} = \frac{\zeta\lambda_0 V_0 c_A + x_{Dy}^2\xi(J_0' - \lambda_0)}{x_{Dy}^2 J_0'(J_0' - \lambda_0)}. \tag{33}$$

The conversion of the quantities $\tilde{\zeta}$ and $\tilde{\xi}$ results from

$$\tilde{\xi} = \zeta\frac{V_0 c_A}{x_{Dy}^2(J_0' - \lambda_0)}. \tag{34}$$

Consideration of the limiting cases $\zeta = 0$ and $\xi = 0$, respectively, shows that anharmonicity of λ for decreasing Dy concentration x_{Dy} gives a greater difference to a non-modified MFA than anharmonicity of the elastic coupling. For $\zeta = 0$, the curves differ less from the MFA curve with increasing Dy dilution. Thus a comparison of the experimental results with the CI model should allow a decision between anharmonicity of the pseudo-spin–pseudo-spin coupling and anharmonicity of the coupling to the macroscopic strain.

4.2.4. CI model and pre-strains. The CI model does not change the calculated transition temperature for given λ_0 and η_0. A diminution of T_D may be explained with the effects described by Bingham *et al* [18] (see § 4.2.1) as well as by pre-strains. The consideration of pre-strains in the CI model requires that the anharmonicity ξ of the distortion operates on the pre-strains, too. In the condition (5) ($\partial F/\partial e_A = 0$), terms proportional to $\int e_v^2 p(e_v)\,de_v$ occur but not in the condition (4) ($\partial F/\partial\langle\sigma^z\rangle = 0$). Hence in the most general case, $\langle\sigma^z\rangle$ and e_A are no longer proportional (see the Appendix). The proportionality is valid only if $\xi = 0$. The two equations for $\langle\sigma^z\rangle$ and e_A then have to be calculated simultaneously with additional parameters (ζ and ξ cannot be converted into each other any more). Furthermore, the solutions are dependent on the ratio of the two interactions. Thus, by incorporating the pre-strains into the CI model, the reasonable limits of an extension of the MFA seem to be reached (or even crossed).

Despite these difficulties we have calculated the distortion and the specific heat, supposing $\xi = 0$ and therefore $\langle\sigma^z\rangle \sim e_A$ for comparison with the experiments (§ 5).

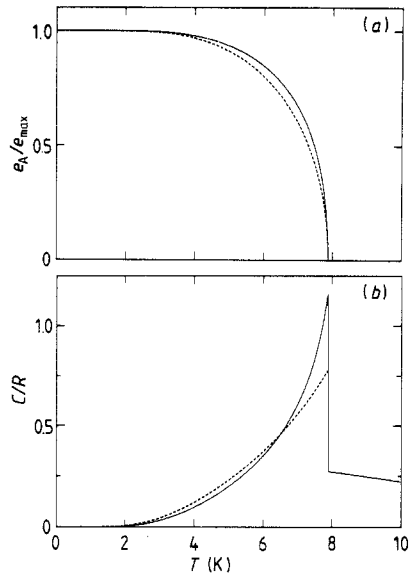

Figure 2. (*a*) Distortion e_A and (*b*) specific heat calculated in the compressible Ising model for a crystal with $x_{Dy} = 0.7$ (i.e. $x = 0.3$) and a Gaussian pre-strain distribution according to equation (20) with $e_{1/2} = 0.0018$ for different values of the compressibility ξ. Full curve: $\xi = 0.200$. Broken curve: $\xi = 0.098$. The distortion has been scaled to its maximum value at $T = 0$.

The possible anharmonicity of η has been considered by a concentration-dependent parameter ξ. The free energy F_{Dy} as a function of e_A only reads

$$F_{Dy}(e_A) = -x_{Dy}kT \int \ln Z_{Dy}[H_0 e_A(1 + \xi e_A^2) + \eta e_v]p(e_v)\,de_v$$
$$+ \tfrac{1}{2}V_0 c_A (J'_{0,Dy}/\mu_{Dy})e_A^2 + \tfrac{3}{4}V_0 c_A \xi e^4 (J'_{0,Dy}/\mu_{Dy}) \qquad (35)$$

where we have dropped a constant proportional to $\int e_v^2 p(e_v)\,de_v$, and the interaction constants H'_0 and η are converted to J'_0 and μ with equation (8). The distortion e_A is calculated self-consistently with equation (5) analogously to equation (23) as well as the energy U_{Dy} and the specific heat.

As mentioned in the last section, a decision between ξ = constant and $\xi \sim x_{Dy}^2$ should be possible from measurements of both the specific heat and the order parameter. For $x = 0.3$ (i.e. $x_{Dy} = 0.7$) the temperature dependence of the order parameter and the specific heat is shown in figure 2 for a half-width $e_{1/2} = 0.0018$ (as was used for the fit of the measured curves; see § 5.3) and different values of the compressibility: $\xi = 0.2$ and $\xi = 0.7^2 \times 0.2$. Order parameter and specific heat are clearly different for these two values of ξ.

5. Experimental results and discussion

5.1. Definition of parameters

In contrast to earlier work on the mixed substances, in this paper both the interaction within the pseudo-spin system and the coupling to elastic strains are considered. For fixed T_D, $\langle\sigma^z\rangle$ and e are proportional and the sum of the corresponding contributions is not changed. This leads to a rescaling of the distortion and the pre-strains compared to earlier publications. Furthermore, the elastic constants for $T \to \infty$ are used instead of

Table 2. General parameters for the mean-field calculations.

Parameter	Reference	$TbVO_4$	$DyVO_4$
$J_0' = \lambda + \mu$ (cm^{-1})	[a]	24.45	10.84
λ/μ	[53]	−0.318	+0.430
ε (cm^{-1})	[50]	9.55	—
ε' (cm^{-1})	[50]	−1.55	—
Δ (cm^{-1})	[49]	—	4.5
$V_0 = \frac{1}{4}V_{tet}$ (nm^3)	[64]	0.0815	0.0806
$c_A = \frac{1}{2}(c_{11} - c_{12})$ ($N\,m^{-2}$)	[53]	[b]	9.95×10^{10}
$c_X = c_{66}$ ($N\,m^{-2}$)	[53]	1.493×10^{10}	[b]
Maximum distortion, $e_0 \times 100$			
calculated		2.32	0.40
measured	[3, 4, 6, 65]	2.24 ± 0.06	0.46 ± 0.04

[a] J_0' was fitted to the transition temperatures of the pure substances. Owing to the slightly smaller transition temperature of $TbVO_4$ in the birefringence (paper II) and spectroscopic measurements, a value of $J_0' = 23.8\,cm^{-1}$ was used for the calculations in these cases.
[b] The elastic constants for $TbVO_4$ and $DyVO_4$ were assumed to be equal.

those for $T = 300$ K, yielding an additional scaling factor. As a whole equations (7) and (22) lead to

$$e = S\tilde{e} = (\mu/J_0')^{1/2}[c_0(300\text{ K})/c(\infty)]^{1/2}\tilde{e} \tag{36}$$

$$e_{1/2} = S_{1/2}\tilde{e}_{1/2} = (J_0'/\mu)^{1/2}[c_0(300\text{ K})/c(\infty)]^{1/2}\tilde{e}_{1/2} \tag{37}$$

with $\tilde{e}$ the distortion for $\mu = J_0'$.

This scaling is only important for the distortion itself and for comparing the half-widths $\tilde{e}_{1/2}$ of the pre-strains in the different publications. The specific heat and the eigenvalues are obviously not changed.

We fitted $J_0' = \lambda + \mu$ to the measured T_D value of the pure substances. For $TbVO_4$, this value and correspondingly the fitted J_0' differs somewhat between specific heat measurements and birefringence (paper II). The ratio λ/μ was taken from Sandercock *et al* [53]. For $DyVO_4$ this is somewhat problematic as Sandercock *et al* consider explicitly short-range interactions. In the present work, the two pseudo-spin contributions ν and $4j$ (equation (34) in [53]) were included in λ. The volume of the unit cell was taken from Schwarz [64]. The calculated maximum distortions are in accordance with those determined from x-ray scattering [3, 4, 6, 65]. In table 2, all used parameters are listed.

For each measured concentration x, the specific heat and the eigenvalues were calculated according to §§ 4.1 and 4.2, respectively. The respective half-widths, $e_{1/2}$ of the pre-strain distribution were fitted to the experimental data. For the Γ_4^+ distorted crystals, the compressibility ζ was an additional fitting parameter. These parameters are listed in table 3.

5.2. Γ_3^+ distorted crystals ($x \geq 0.4$)

5.2.1. Specific heat. As in the mixed system $(Tb_x,Tm_{1-x})VO_4$ [19], the Γ_3^+ transition in the Tb-rich compounds ($0.4 \leq x \leq 1.0$) of $(Tb_x,Dy_{1-x})VO_4$ shows almost perfect mean-field behaviour, i.e. the specific heat curves are triangular-shaped. In figure 3, measured and calculated specific heat curves are compared for $x = 0.8$ and $x = 0.6$. The Dy

Table 3. Fit parameters for the calculations on the diluted substances: $e_{1/2}$ is defined in equation (20*a*), $\tilde{\zeta}$ in equation (32). Because of clearer representation, e_s is not listed ($0 \leq e_s \leq 6 \times 10^{-6}$ in all calculations). $e_{1/2}$ and e_s have the same symmetry as the corresponding distortion, e_X and e_A respectively. For comparison, $e_{1/2}$ for $(Tb_x,Tm_{1-x})VO_4$ and $(Tb_x,Yb_{1-x})VO_4$ [20] with a scaling according to equation (37) are given.

Γ_3^+ distorted crystals

	$e_{1/2} \times 100$		
	$(Tb_x,Dy_{1-x})VO_4$		$(Tb_x,Tm_{1-x})VO_4$/ $(Tb_x,Yn_{1-x})VO_4$
Tb concentration, x	Specific heat (this paper)	Birefringence (paper II) and spectroscopy (this paper)	Birefringence [20]
1.0	0.0	0.0	0.0
0.9	0.09	0.10	0.44
0.8	0.21	0.25	0.51
0.71[a]	0.0	0.0	0.69
0.6	0.25	0.23	0.71
0.5	0.33	0.27	0.62
0.45	—	0.24	0.65
0.4[b]	0.27	0.26	—
0.35	—	0.19	—

Γ_4^+ distorted crystals

	$e_{1/2} \times 100$		
	Specific heat, spectroscopy (this paper) and birefringence (paper II)	ζ	
Tb concentration, x		Specific heat and spectroscopy (this paper)	Birefringence (paper II)
0.0	0.0	0.2	0.265
0.1	0.063	0.2×0.9^2	0.265
0.2	0.148	0.2×0.8^2	0.240
0.3	0.180	0.2×0.7^2	0.265
0.35	0.213	—	0.265
0.4[c]	0.199	0.2×0.6^2	—
0.4[d]	0.177	0.257×0.6^2	0.340
0.45[e]	0.200	—	0.265

[a] Nominal concentration (see text).
[b] The calculations for the two measured samples were fitted with the same parameters $e_{1/2}$ and e_s.
[c] Sample I (see § 5.3.2).
[d] Sample II (see § 5.3.2).
[e] No phase transition was observed. Despite this, in a finite magnetic field a birefringence was observed and the measured birefringence curves were fitted with these parameters.

contribution to the specific heat is shown, too. The fits are in reasonable agreement with the measurements, although the jumps at the phase transition differ somewhat. The jump of the specific heat is slightly smeared out with decreasing Tb concentration. This

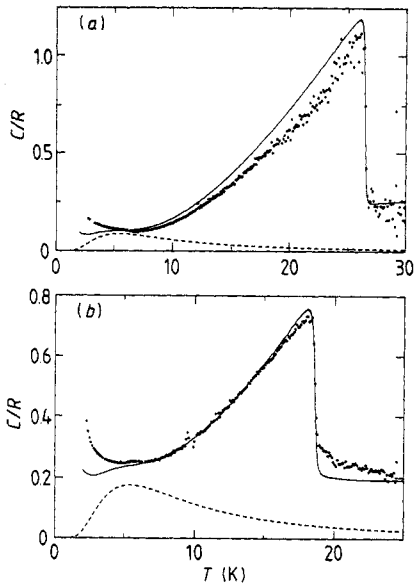

Figure 3. Molar specific heat of $(Tb_x,Dy_{1-x})VO_4$. The lattice contribution and the contributions of sample holder, heater and thermometer have been subtracted. (*a*) $(Tb_{0.8},Dy_{0.2})VO_4$; (*b*) $(Tb_{0.6},Dy_{0.4})VO_4$. Dots: experimental results. Full curve: calculated in MFA with pre-strains according to § 4.1.2. The parameters for the calculations are listed in tables 2 and 3. Broken curve: Dy contribution to the specific heat (included in the full curve).

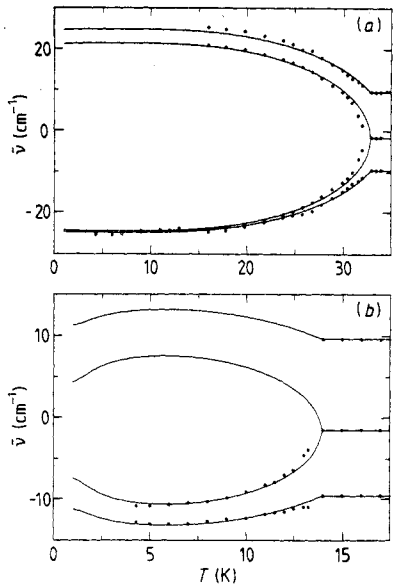

Figure 4. Energy of the four lowest $^7F_6$ levels of the Tb^{3+} ion in $(Tb_x,Dy_{1-x})VO_4$ for (*a*) $x = 1.0$ and (*b*) $x = 0.5$ compared with the MFA calculations (parameters of table 3). Dots: experimental results. Full curves: calculation.

smearing-out was more pronounced in $(Tb_x,Tm_{1-x})VO_4$ and $(Tb_x,Tm_{1-x})AsO_4$ [19]. It may be expressed phenomenologically by an increase of the unsymmetrical part of the pre-strain distribution with the parameter e_s (§ 4.1.2).

5.2.2. Spectroscopy. The Tb ground state determined from $^7F_6 \rightarrow {}^5D_4$ transitions shows mean-field behaviour for $0.5 \leqslant x \leqslant 1.0$ (figure 4). For the first time, measurements for pure $TbVO_4$ over the whole temperature range are presented. For $x \leqslant 0.8$, the upper singlet could not be determined experimentally, and for $x \leqslant 0.6$ the upper doublet component could not be detected either. For $x < 0.3$ no change in the energy of the levels was observed. The Tb^{3+} ion in the vanadate lattice does not couple to Γ_4^+ distortions [9]. Although for $x = 0.3$ and $x = 0.4$ the spectra showed some temperature-dependent change, the ground state could not be determined from the measurements because of the low contrast and the lack of sharpness of the lines.

5.3. Γ_4^+ distorted crystals ($x \leqslant 0.4$)

5.3.1. Spectroscopy. The distance of the two lowest Kramers doublets of the Dy ground state, determined from $^6H_{15/2} \rightarrow {}^4F_{9/2}$ transitions, is shown in figure 5 for $x \leqslant 0.3$. The

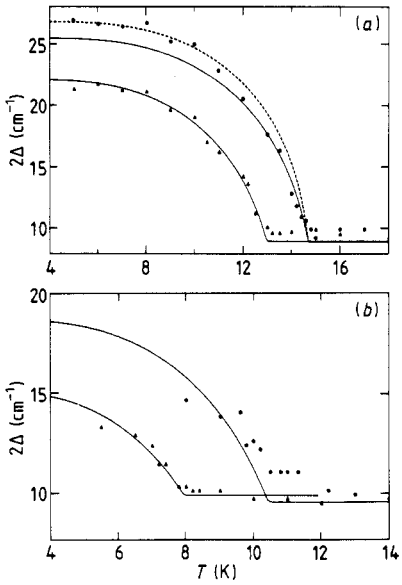

Figure 5. Distance 2Δ of the two lowest $^6H_{15/2}$ Kramers doublets of the Dy^{3+} ion in $(Tb_x,Dy_{1-x})VO_4$ compared with the CI model calculation including pre-strains according to § 4.2.4 (parameters of table 3). Full curve: fit with $\tilde{\xi} = 0.20x_{Dy}$. Broken curve: fit with $\tilde{\xi} = 0.265$. (*a*) Pure $DyVO_4$ (dots) and $(Tb_{0.1}, Dy_{0.9})VO_4$ (triangles). (*b*) $(Tb_{0.2},Dy_{0.8})VO_4$ (dots) and $(Tb_{0.3},Dy_{0.7})VO_4$ (triangles).

maximum distance $2\Delta_{max}$ at low temperatures decreases with decreasing Dy concentration because of less effective coupling between the Dy^{3+} ions. Furthermore, for $x \geqslant 0.5$, no change in the energy of the levels was observed, so the Dy^{3+} ion in the vanadate lattice does not couple to Γ_3^+ distortions [9]. It was therefore surprising that for $x = 0.4$ both transitions are discernible in the spectrum and that the Γ_3^+ distortion seems to act in some way on the ground state. The distance 2Δ is increasing with decreasing temperature even in the range $T_{D2} \leqslant T \leqslant T_{D1}$ and $2\Delta_{max}$ is greater for $x = 0.4$ than for $x = 0.3$. Though the reasons for an interaction of the Γ_3^+ distortion on the Dy^{3+} levels remain unclear, this distortion must produce or enhance an inherent Γ_4^+ or Γ_1^+ stress (or a stress of other symmetry), possibly caused by insufficient crystal quality. With the crystal-field splitting, $2\Delta_0$, the additional splitting for $T_{D2} \leqslant T \leqslant T_{D1}$, $2\Delta_1(T)$, and the splitting due to the Jahn–Teller Γ_4^+ distortion, $2\Delta_2(T)$, the total splitting, 2Δ, as a function of T can be written as

$$2\Delta(T) = 2[\Delta_0^2 + \Delta_1^2(T) + \Delta_2^2(T)]^{1/2} \tag{38}$$

if $\Delta_1(T)$ is caused by a stress with symmetry different from Γ_4^+, or as

$$2\Delta(T) = 2\{\Delta_0^2 + [\Delta_1(T) + \Delta_2(T)]^2\}^{1/2} \tag{39}$$

if $\Delta_1(T)$ is caused by a Γ_4^+ stress. From stress-dependent measurements on $DyVO_4$ [49] a Γ_4^+ stress that would be responsible for the observed change of 2Δ in this temperature region can be estimated to be 200 MPa. With the measured elastic constant $\frac{1}{2}(c_{11} - c_{12})$ [53], this corresponds to an (inhomogeneous) Γ_4^+ strain of $e_{max} \simeq 0.2\%$.

The eigenvalues calculated in the CI modification of the MFA are in accordance with the spectroscopic measurements using the same parameters as for the specific heat (see below). Though a decision between $\tilde{\xi} = 0.2$ and $\tilde{\xi} = 0.265$ (or a value in between) cannot be made, the energy eigenvalues clearly deviate from pure mean-field behaviour ($\tilde{\xi} = 0$); see figure 5(*a*). Furthermore, $\tilde{\xi}$ shows the same dependence on the concentration as for the specific heat. In the calculation the greater width of the pre-strain distribution

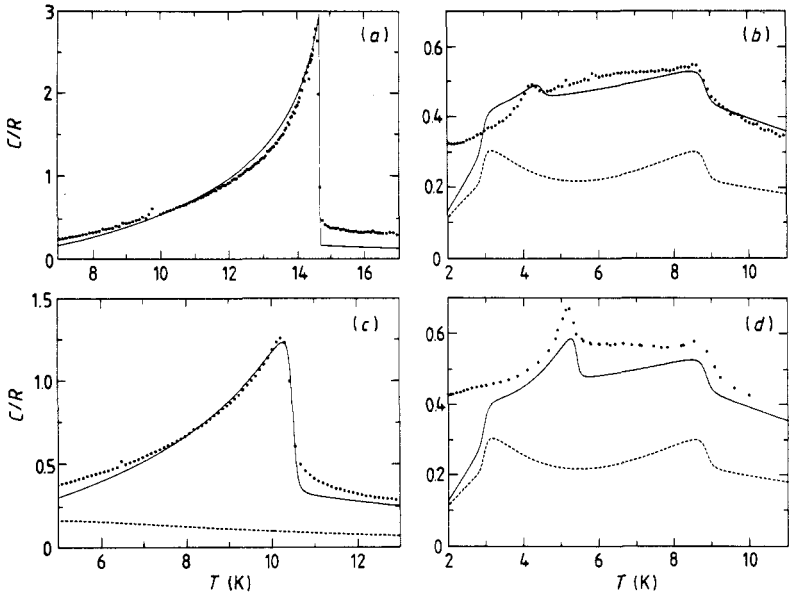

Figure 6. Molar specific heat of $(Tb_x,Dy_{1-x})VO_4$. The lattice contribution and the contributions of sample holder, heater and thermometer have been subtracted. Dots: experimental results. Full curve: calculated in the CI model with pre-strains according to § 4.2.4 (parameters of table 3). Broken curve: Tb contribution to the specific heat (included in the full curve). (*a*) Pure $DyVO_4$; (*b*) $(Tb_{0.4},Dy_{0.6})VO_4$, sample I; (*c*) $(Tb_{0.2},Dy_{0.8})VO_4$; (*d*) $(Tb_{0.4},Dy_{0.6})VO_4$, sample II (this sample was used for the birefringence measurements in paper II).

for increasing dilution clearly affects the mean distance between the two Kramers doublets for $T > T_D$ (figure 5(*b*)). In the experiments, however, this shift due to internal strains cannot be detected.

5.3.2. Specific heat. In contrast to the Tb-rich compounds, the Dy-rich compounds ($0.0 \leqslant x \leqslant 0.3$) show λ-shaped behaviour. This is due to dominant short-range Jahn–Teller interactions via optical phonons (e.g. [53]). The maximum value of the specific heat of pure $DyVO_4$ (figure 6(*a*)) is much smaller than in earlier publications [12, 66] (this is most probably caused by insufficient consideration of thermal noise, which reduces the measured specific heat, especially around the phase transition where the measuring time is long). With decreasing Dy concentration the measured curves (figure 6(*c*)) are less concave for $T < T_D$, indicating a smaller deviation from mean-field behaviour. Additionally the high-temperature tail, which is even present in pure $DyVO_4$, becomes more distinct. While in pure $DyVO_4$ this tail was attributed to random strains [12], for the diluted substances this explanation is questionable (see below). By 'high-temperature tail' we do not mean the tail of the Schottky anomaly of a two-level system, which is naturally present in diluted $DyVO_4$, too, but the strong smearing-out of the jump of the specific heat for $T > T_D$. For $x = 0.3$, for example, this tail exists up to $T \simeq 1.2T_D$ (figure 7).

At low temperatures $DyVO_4$ shows a magnetic phase transition from the paramagnetic high-temperature phase to an antiferromagnetic phase [66, 67]. This phase

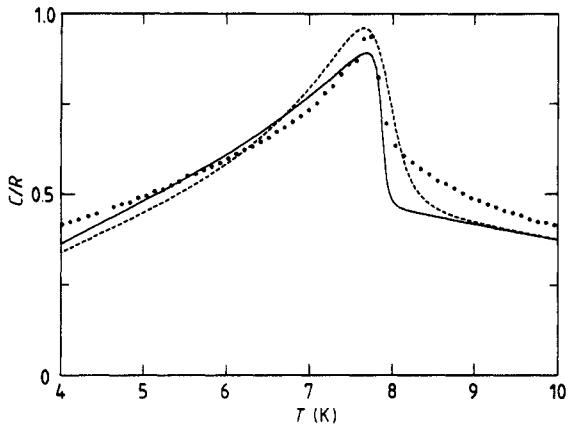

Figure 7. Comparison of the measured specific heat of $(Tb_{0.3},Dy_{0.7})VO_4$ (lattice contribution and contributions of sample holder, heater and thermometer subtracted) with calculations in the CI model with different parameters. Dots: experimental results. Full curve: $e_{1/2} = 0.00185$, $e_s = 7 \times 10^{-6}$, $\tilde{\xi} = 0.200$. Broken curve: $e_{1/2} = 0.00180$, $e_s = 10^{-6}$, $\tilde{\xi} = 0.098$.

transition could be observed in the mixed substances for $x \leqslant 0.5$ (table 1). Its high-temperature tail is still found for $x = 0.6$ (figure 3(*b*)). For greater Dy dilution, it is below the experimental limit of 1.1 K.

For $x = 0.4$ both structural transitions are observed (figures 6(*b*) and (*d*)). For this concentration two different samples grown in different batches were investigated. The upper transition temperature, corresponding to the Γ_3^+ transition of diluted $TbVO_4$, is identical within the experimental accuracy. The lower transition temperature, corresponding to the Γ_4^+ transition of diluted $DyVO_4$, however, differs remarkably for the two samples. Because their Néel temperatures are nearly the same, this cannot be due to a different Dy concentration, but may be an effect of lesser crystal quality of the sample shown in figure 6(*b*) causing stronger random strains.

For pure $DyVO_4$ the specific heat can be fitted best with a compressibility $\tilde{\xi} = 0.2$ (figure 6(*a*)). The difference from Page *et al* [12], who obtained $\tilde{\xi} = 0.25$, results from the smaller jump of the specific heat in our experiments. With other methods, the following parameters $\tilde{\xi}$ have been fitted: 0.15 (dielectric constant, [13]) and 0.265 (birefringence, [11] and paper II). The specific heat of the diluted substances was fitted according to § 4.2.4. The best fit for these substances is achieved with $\tilde{\xi}(x) = x_{Dy}^2 \tilde{\xi}(x_{Dy} = 1)$ (figures 6(*b*) to (*d*)). For the second measured sample with $x = 0.4$, a somewhat greater value fits the measured curve better. The Tb contribution to the specific heat is also shown in the figures. For the samples with $x = 0.4$, this contribution is not only due to the specific heat of an unchanged four-level system, as for the samples with $x \leqslant 0.3$, but is altered by the Γ_3^+ distortion. For $T \leqslant 2.8$ K this distortion should disappear again. Because of the vicinity of the magnetic phase transition for these temperatures, a comparison of calculations and experiments does not seem to be reasonable.

The good agreement of the compressibility fitted to the specific heat and fitted to the spectroscopic measurements, despite the theoretical restrictions of § 4.2.4, makes it plausible that the compressibility arises from an anharmonic term in the strain and not in the pseudo-spin–pseudo-spin coupling. This contradicts the fit of the birefringence (paper II), where $\tilde{\xi}(x_{Dy}) \approx$ constant was obtained (table 3). It is important that this discrepancy exists for measurements on the same sample ($x = 0.4$, sample II). Although the birefringence in the diluted substances does not necessarily reveal the temperature dependence of the distortion (because of an eventual Tb contribution that requires at

least one new free parameter), we do not believe that this effect is the main cause for the difference in the compressibility. Although the calculations fit the specific heat well, there nevertheless remain some unsolved questions. The measured curve of $(Tb_{0.3},Dy_{0.7})VO_4$, for example (figure 7), is more concave than the calculated curve. Therefore a fit was tried with $\tilde{\xi} = 0.2$ (i.e. the value of $DyVO_4$) and a relatively high value of e_s, the unsymmetrical part of the pre-strain distribution (equation (20*a*)), in order to reduce the height of the peak in the calculated curve with $e_s = 0$ (figure 2(*b*)). The result is shown in figure 7. Altogether, this calculation agrees less well with the experiment than the former calculation. In the surroundings of T_D the curve calculated in this way is broader than the observed one. The slope of the specific heat indeed becomes less steep for increasing values of e_s, but for this modification the high-temperature behaviour as a whole is not reproduced.

The CI model and every modification of it are modified mean-field approximations and are therefore based on long-range interactions. Although the CI model gives satisfactory results for pure substances with short-range interactions, this is not a consequence of an explicit consideration of the short-range character. For the diluted substances, this deficiency becomes more distinct and makes such sophisticated attempts as the unsymmetrical random pre-strain distribution in the CI modification of the MFA questionable. Nevertheless, theories that consider the short-range interactions in diluted substances and go beyond effective-field approximations do not exist to our knowledge. This is true both for diluted ferroelastics and for the analogous case of diluted Ising ferromagnets. It seems worth mentioning that the case of diluted $DyVO_4$ is even more complicated than an ordinary diluted Ising ferromagnet, both because of the finite crystal-field splitting for $T > T_D$ and because there are also long-range interactions present due to the coupling to elastic strains and to the coupling via acoustic phonons.

6. Summary

Measurements of specific heat, birefringence and optical spectroscopy established the phase diagram and the transition temperatures of the mixed Jahn–Teiler system $(Tb_x,Dy_{1-x})VO_4$. The behaviour of the mixed substances for the Tb-rich compounds is determined by the characteristics of pure $TbVO_4$ and for the Dy-rich compounds by those of pure $DyVO_4$. For intermediate concentrations $x = 0.35$ and $x = 0.4$, crystal optical investigations show a superposition of the two different distortion types of the pure substances.

According to the undisturbed superposition of the two distortion types, the values of the distortions can be calculated independently. For the mixed substances distorting like $TbVO_4$, a mean-field calculation with the inclusion of random pre-strains explains the measured curves very well. For the mixed substances distorting like $DyVO_4$, an extension of the mean-field approximation by the compressible Ising model including random pre-strains was necessary to get a good agreement between calculations and experimental findings. The agreement is not quite as satisfactory as for the substances distorting like $TbVO_4$. This is caused by the superposition of long-range and short-range Jahn–Teller interactions in the Dy compounds. In this paper a large amount of experimental results have been presented where the theoretical interpretation is not yet fully satisfactory. Further effort, mainly from a theoretical point of view, would be desirable to get a more distinct understanding.

Acknowledgments

The authors wish to thank Dr W Wendl of the Kristall- und Materiallabor der Fakultät für Physik der Universität Karlsruhe for growing the crystals and Dr M Schienle, Dr J Wosnitza, Dr J Hoffmann and P Oreans for experimental assistance. The computer calculations were performed at the VAX 11/750 der Fakultät für Physik der Universität Karlsruhe.

Appendix

For diluted $DyVO_4$, in the general case, a pseudo-spin–pseudo-spin coupling (λ_0), a coupling of the pseudo-spins to the macroscopic strain (η_0), different anharmonicities (ζ and ξ) for these two interactions and an additonal pre-strain (e_v) have to be taken into account. In the CI model, the partition function Z_{Dy} of the Dy^{3+} ion

$$Z_{Dy} = Z_{Dy}(y) = Z_{Dy}\{x_{Dy}\lambda_0\langle\sigma^z\rangle(1 + \zeta\langle\sigma^z\rangle^2) + \eta_0(e_A + e_v)[1 + \xi(e_A + e_v)^2]\} \tag{A1}$$

is a function of y with

$$y = x_{Dy}\lambda_0\langle\sigma^z\rangle(1 + \zeta\langle\sigma^z\rangle^2) + \eta_0(e_A + e_v)[1 + \xi(e_A + e_v)^2]. \tag{A2}$$

Then according to equations (21) and (30) and the pre-strain distribution equation (20), the free energy F_{Dy} reads

$$F_{Dy}(\langle\sigma^z\rangle, e_A) = -x_{Dy}kT\int \ln Z_{Dy}(y)p(e_v)\,de_v + \tfrac{1}{2}x_{Dy}^2\lambda_0\langle\sigma^z\rangle^2 + \tfrac{3}{4}x_{Dy}^2\zeta\lambda_0\langle\sigma^z\rangle^4$$

$$+\tfrac{1}{2}V_0c_A\int(e_A+e_v)^2p(e_v)de_v+\tfrac{3}{4}V_0c_A\xi\int(e_A+e_v)^4p(e_v)de_v. \tag{A3}$$

The conditions for thermal equilibrium, equations (4) and (5), yield

$$\langle\sigma^z\rangle = kT\int\frac{1}{Z_{Dy}(y)}\frac{\partial Z_{Dy}(y)}{\partial y}p(e_v)\,de_v \tag{A4}$$

and

$$e_A\left(1 + 9\xi\int e_v^2p(e_v)\,de_v\right) + 3\xi e_A^3$$

$$= x_{Dy}kT\frac{\eta_0}{V_0c_0}\int\frac{1}{Z_{Dy}(y)}\frac{\partial Z_{Dy}(y)}{\partial y}[1 + 3\xi(e_A + e_v)^2]p(e_v)\,de_v. \tag{A5}$$

Obviously $\langle\sigma^z\rangle$ and e_A are only proportional if either $\xi = 0$ or there are no pre-strains. In these special cases equation (6) is still valid. In the general case, however, both equations (A4) and (A5) have to be solved simultaneously. Then the solutions are dependent not only on ζ and ξ but also on the ratio λ_0/η_0 of the coupling constants. The transition temperature thus depends not only on the half-width $e_{1/2}$ but also on ζ and ξ.

References

[1] Gehring G A and Gehring K A 1975 *Rep. Prog. Phys.* **38** 1–89

[2] Wyckoff R W G 1965 *Crystal Structures* vol. 3 (New York: Interscience)
[3] Göbel H and Will G 1972 *Phys. Status Solidi* b **150** 147–54
[4] Göbel H and Will G 1972 *Int. J. Magn.* **3** 123–8
[5] Sayetat F 1972 *Solid State Commun.* **10** 879–82
[6] Will G, Göbel H, Sampson C F and Forsyth J B 1972 *Phys. Lett.* **38A** 207–8
[7] Nye J F 1985 *Physical Properties of Crystals* (Oxford: Clarendon)
[8] Gehring K A, Malozemoff A P, Staude W and Tyte R N 1971 *Solid State Commun.* **9** 511–14
[9] Elliott R J, Harley R T, Hayes W and Smith S R P 1972 *Proc. R. Soc.* A **328** 217–66
[10] Harley R T and Macfarlane R M 1975 *J. Phys. C: Solid State Phys.* **8** L451–5
[11] Gehring G A, Harley R T and Macfarlane R M 1980 *J. Phys. C: Solid State Phys.* **13** 3161–74
[12] Page J H and Taylor D R 1981 *Solid State Commun.* **40** 907–9
[13] Page J H, Taylor D R and Smith S R P 1984 *J. Phys. C: Solid State Phys.* **17** 51–71
[14] Glynn T J, Harley R T and Macfarlane R M 1977 *J. Phys. C: Solid State Phys.* **10** 2937–46
[15] Harley R T, Hayes W, Perry A M, Smith S R P, Elliott R J and Saville I D 1974 *J. Phys. C: Solid State Phys.* **7** 3145–60
[16] Gehring G A, Swithenby S J and Wells M R 1976 *Solid State Commun.* **18** 31–4
[17] Schwab M 1978 *Phys. Status Solidi* b **86** 195–203
[18] Bingham D, Morgan M J and Cashion J D 1984 *Proc. R. Soc.* A **391** 85–107
[19] Kasten A, Kahle H G, Klöfer P and Schäfer-Siebert D 1987 *Phys. Status Solidi* b **144** 423–36
[20] Pilawa B, Hess G, Kahle H G and Kasten A 1988 *Phys. Status Solidi* b **145** 729–39
[21] Taylor D R, Zwartz E, Page J H and Watts B E 1986 *J. Magn. Magn. Mater.* **54–57** 57–8
[22] Graham J T, Maliepaard M, Page J H, Smith S R P and Taylor D R 1987 *Phys. Rev.* B **35** 2098–101
[23] Hess G 1989 *J. Phys.: Condens. Matter* **2** 1097
[24] Hess G, Hikel W and Kahle H G 1989 *J. Phys.: Condens. Matter* **2** 1113
[25] Hess G and Kahle H G 1988 *J. Physique Suppl.* **49** C8 891–2
[26] Hintzmann W and Müller-Vogt G 1969 *J. Crystal Growth* **5** 274–8
[27] Wahlstrom E E 1979 *Optical Crystallography* (New York: Wiley)
[28] Gehring K A and Rosenberg H M 1971 *Phys. Status Solidi* b **47** K75–8
[29] Kasten A and Becker P J 1973 *Int. J. Magn.* **5** 157–60
[30] Leask M J M, Maxwell K J, Tyte R N, Becker P J, Kasten A and Wüchner W 1973 *Solid State Commun.* **13** 693–5
[31] Kasten A, Berndts P and Kahle H G 1975 *Physica* **80B** 258–68
[32] Hess G 1988 *Doctoral Thesis* Universität Karlsruhe
[33] Hikel W, Hess G and Kahle H G 1989 *J. Phys.: Condens. Matter* **1** 2137–40
[34] Wold A, Arnott R J, Whipple E and Goodenough J B 1963 *J. Appl. Phys.* **34** 1085–6
[35] Kino Y and Miyahara S 1966 *J. Phys. Soc. Japan* **21** 2732
[36] Inaba H, Yagi H and Naito K 1986 *J. Solid State Chem.* **64** 67–75
[37] Ito A 1986 *Hyperfine Interactions* **33** 89–103
[38] Aharony A and Fishman S 1976 *Phys. Rev. Lett.* **37** 1587–90
[39] Matsubara F and Inawashiro S 1977 *J. Phys. Soc. Japan* **42** 1529–37
[40] Kanamori J 1960 *J. Appl. Phys.* **31** 14–23S
[41] Kataoka M and Kanamori J 1972 *J. Phys. Soc. Japan* **32** 113–34
[42] Aharony A 1975 *Phys. Rev. Lett.* **34** 590–3
[43] Liu K S and Fisher M E 1973 *J. Low Temp. Phys.* **10** 655–83
[44] Katsumata K, Kobayashi M, Satō T and Miyako Y 1979 *Phys. Rev.* B **19** 2700–3
[45] Katsumata K, Kobayashi M and Yoshizawa H 1979 *Phys. Rev. Lett.* **43** 960–3
[46] Katsumata K, Yoshizawa H, Shirane G and Birgeneau R J 1985 *Phys. Rev.* B **31** 316–20
[47] Wong P, Horn P M, Birgeneau R J, Safinya C R and Shirane G 1980 *Phys. Rev. Lett.* **45** 1974–7
[48] Wong P, Horn P M, Birgeneau R J and Shirane G 1983 *Phys. Rev.* B **27** 428–47
[49] Gehring G A, Malozemoff A P, Staude W and Tyte R N 1972 *J. Phys. Chem. Solids* **33** 1499–510
[50] Gehring G A, Kahle H G, Nägele W, Simon A and Wüchner W 1976 *Phys. Status Solidi* b **74** 297–309
[51] McPherson J W and Wang Yung-Li 1975 *J. Phys. Chem. Solids* **36** 493–9
[52] Pytte E 1974 *Phys. Rev.* B **9** 932–41
[53] Sandercock J R, Palmer S B, Elliott R J, Hayes W, Smith S R P and Young A P 1972 *J. Phys. C: Solid State Phys.* **5** 3126–46
[54] Wells M R and Worswick R D 1972 *Phys. Lett.* **42A** 269–71
[55] Imry Y and Ma S K 1975 *Phys. Rev. Lett.* **35** 1399–401
[56] Aharony A, Imry Y and Ma S K 1976 *Phys. Rev. Lett.* **37** 1364–7

[57] Harley R T, Perry C H and Richter W 1977 *J. Phys. C: Solid State Phys.* **10** L187–9
[58] Schneider T and Pytte E 1977 *Phys. Rev.* B **15** 1519–22
[59] Sherrington D and Kirkpatrick S 1975 *Phys. Rev. Lett.* **35** 1792–6
[60] Klein M W, Schowalter L J and Shukla P 1979 *Phys. Rev.* B **19** 1492–502
[61] Page J H, Smith S R P, Taylor D R and Harley R T 1979 *J. Phys. C: Solid State Phys.* **12** L875–81
[62] Domann G, Kahle H G, Kasten A and Schwarzbauer H J 1980 *J. Magn. Magn. Mater.* **15–18** 37–8
[63] Smith S R P 1984 *J. Phys. C: Solid State Phys.* **17** 41–50
[64] Schwarz H 1963 *Z. Anorg. Allg. Chem.* **323** 44–56
[65] Smith S R P and Tanner B K 1978 *J. Phys. C: Solid State Phys.* **11** L717–20
[66] Cooke A H, Martin D M and Wells M R 1971 *Solid State Commun.* **9** 519–22
[67] Kasten A 1980 *Z. Phys.* B **38** 65–76